International Journal of Control, Automation and Systems 19(12) (2021) 3967-3982
http://dx.doi.org/10.1007/s12555-020-0292-1
ISSN:1598-6446 eISSN:2005-4092
http://www.springer.com/12555

Nonlinear Anti-swing Control of Underactuated Tower Crane Based on Improved Energy Function

Huai-Tao Shi, Jian-Qi Huang, Xiaotian Bai*, Xiang Huang, and Jie Sun

Abstract: The control system of tower crane exhibits strong nonlinearity in the process of control execution, which is prone to the problems of inaccurate positioning control of the payload and difficult anti-swing control. Aiming at the problems, this paper proposes a control law based on improved energy coupling analysis for suppressing the payload swing in the tower cranes. A three-dimensional dynamic model of tower crane system with considering friction is established, and an improved energy coupling signal is designed. The coupling relationship of trolley movement and payload swing, jib rotation and payload swing are considered, then a nonlinear anti-swing controller is established in order to reduce the swing. The closed-loop stability of the system with the controller is verified by the Lyapunov method and LaSalle invariance principle, simulations and experimental analyses are performed to verify the controller performance. The control performance of the controller is compared with other classic and typical current control methods, and the proposed controller outperformed other controllers. The anti-swing controller proposed in this paper has accurate positioning, and can achieve precise control when the payload is transported, reaching the set target position in a little time and eliminating residual swing angle. Meanwhile the proposed controller has a good control robustness, which can restore stability in around a very short time when the rope length and payload mass of the system's inherent property are changed and external interference is added. In addition, when different target position parameters are uncertain, the proposed control law has good robust performance.

Keywords: Energy coupling, nonlinear dynamic model, tower crane, underactuated system.

1. INTRODUCTION

As a typical hoisting engineering machine widely used in construction sites, tower crane is mainly used for accurate and rapid point-to-point lifting, transporting and lowering of materials to designated positions. Tower crane needs to prevent the payload from swinging substantially during the transporting process [1]. The control system of tower crane is a typical underactuated system because its inputs is less than the number of system degrees of freedom. The control system exhibits a strong nonlinearity in the process of control execution, so it is a nonlinear underactuated system. This type of control system is susceptible to various external interference, so it is difficult to achieve the expected effect quickly and accurately. During the transporting process, the payload is prone to large swings, affecting the system transporting payload positioning accuracy and great security risks [2]. On the other hand, when the payload mass and length of rope change, a large difference occurs during the positioning of the system, which affects the control robustness of the system. Therefore, solving the problem of tower crane's payload accurate positioning, swing amplitude suppression and control robustness has become an important problem in the precise control of construction machinery at present.

The core problem of underactuated crane control is to establish nonlinear model and the design of the anti-swing control law. At present, most scholars have done lots of research on the automatic control system of underactuated overhead cranes. There are both traditional open-loop control methods without state feedback [3], and closed-loop control methods with state feedback [4–9]. These control methods are of great significance for studying anti-swing control of nonlinear underactuated tower cranes. For un-

Manuscript received April 28, 2020; revised October 14, 2020 and January 13, 2021; accepted March 4, 2021. Recommended by Associate Editor Aldo Jonathan Munoz-Vazquez under the direction of Editor Jay H. Lee. This research was supported by National Science Foundation of China under Grant 52075348, Science&technology planning project of MOHURD under Grant 2019-K-080, Key R&D Program of Hebei Province under Grant 19211904D, Key science and technology research project of Shenyang under Grant 20-202-4-40, and Key innovate R&D Program of Shenyang under Grant Y19-1-004.

Huaitao Shi, Jianqi Huang, and Xiaotian Bai are with the School of Mechanical Engineering, Shenyang Jianzhu University, Shenyang 110168, China (e-mails: sht@sjzu.edu.cn, h_jq@stu.sjzu.edu.cn, baixt@sjzu.edu.cn). Xiang Huang is with Key Lab E&M, Zhejiang University of Technology, Hangzhou 310014, China (e-mail: oscarhx@zjut.edu.cn). Jie Sun is with The State Key Laboratory of Rolling and Automation, Northeastern University, Shenyang 110819, China (e-mail: sunjie@ral.neu.edu.cn).
* Corresponding author.

deractuated tower crane nonlinear systems, its dynamic characteristics are complex. First of all, the tower crane has a rotary motion of the jib, which is no longer a single linear motion in two directions. This creates more complex structural characteristics. The coupling of the jib rotation and payload swing leads to the increased difficulties of controller analysis and design of tower crane. The control of coupling the payload swing with the movement of the jib and the trolley in the nonlinear system of the tower crane is more difficult and challenging [10–12].

For the control method of nonlinear underactuated tower cranes, the predecessors have done a lot of research work. In order to minimize the swing of the payload, Omar and Nayfeh developed a tower crane system control scheme based on dispatch feedback and fuzzy feedback [13–15]. The controller can lift the payload within one oscillation period of the payload without causing overshoot for the trolley position. In the process of transporting payload, the transporting payload time is close to the optimal time, and it is small for the payload swing angle. Vermeiren and Gonzalez *et al.* extended linear control theory to robust control theory by introducing uncertainty. Fuzzy control and gain scheduling control based on the LPV method are one of the effective methods to solve the control problem of nonlinear systems, and achieve good control effect [16,17]. However, the introduction of uncertainty in the design process will cause the performance of the designed controller to decline. In addition, multiple controllers are designed, and the controller is switched according to the parameter change trajectory to realize the gain scheduling control, which effectively solves the control problem of the system with sector nonlinear input, parameter uncertainty and external noise interference [18], but its dynamic characteristics depend on real-time measurable adjustment parameters. In [19], Vaughan *et al.* shaped the reference command according to the system's natural frequency, developed and utilized the control method on the basis of command shape to reduce the swing of the tower crane's payload. However, the reference for the controllers is generally a step input, which causes them fitter for short distances. Another problem of the controllers is the sudden change of control action at the starting of the movement, causing huge shocks. Furthermore, the adjustment algorithm has not been tested experimentally. Duong *et al.* designed a control strategy for underactuated tower crane systems based on recurrent neural networks, and used hybrid evolutionary algorithms to further improve the overall control performance [20]. Wu and Sun, *et al.* put forward an adaptive fuzzy control scheme to improve the performance of tower crane and effectively suppress payload swing, and the traditional LQR controller with excellent control effect in the optimal control and the adaptive trajectory tracking controller(ATTC) is also applied to the control system of the tower crane [21–25]. But this method is slower to eliminate the residual swing angle when the system tends to stabilize. In [26–28], Lee *et al.* designed a control method based on adaptive synovial control and adaptive neural control. Le *et al.* improved the controller under the adaptive layered sliding mode control strategy founded on neural network, which improved the adaptive performance of payload swing [29]. For the purpose of controlling the robustness of tower crane system, Coral-Enriquez *et al.* reduced the robustness of the system based on the extended state resonance observer control scheme [30]. However, these controllers have complex features and are hard to apply in the actual three-dimensional transporting process of a tower crane. And friction is not considered in most models. In practical system, friction has a great influence on system performance, which should be incorporated into the design of controller. In [31], El-Badawy *et al.* proposed an inverse dynamics control scheme and carried out experimental verification. In [32], Koumboulis *et al.* used a model to change the friction compensation method to complete the control task. In [33], Lee *et al.* developed a tower crane trajectory tracking system based on laser and verified its effectiveness. Bock *et al.* proposed a new model predictive control method, which makes the payload move along a predetermined path by ignoring certain specific terms to complete the control task [34]. However, these control methods are very sensitive to external interference and parameter changes.

Aiming at the above problems, this paper designs a control law for tower cranes based on improved energy coupling analysis. The constructed nonlinear anti-swing controller effectively controls the positioning of the jib and the trolley, payload swing and swing amplitude suppression. Then, the system's closed-loop stability under the control law is verified by Lyapunov method and LaSalle invariance principle. Finally, the designed controller is analyzed by simulation and applied to the experimental platform verified the actual performance of the controller.

The organizational structure of the article is as follows: In Section 2, the tower crane dynamics model's mathematical description is established and the relationship between the parameters in the model is analyzed in detail. Then in the third section, the design of the controller and stability analysis are carried out taking the above model as the basis. We design the controller based on improved energy coupling and its stability is verified by Lyapunov method and LaSalle invariance principle. In the fourth section, simulation analysis and experimental verification of the control effect are carried out. Finally, the full text is summarized in Section 5.

2. ESTABLISHMENT OF SYSTEM MODEL

The schematic diagram of the three-dimensional model of payload swing during the transporting process of the tower crane can be described as Fig. 1.

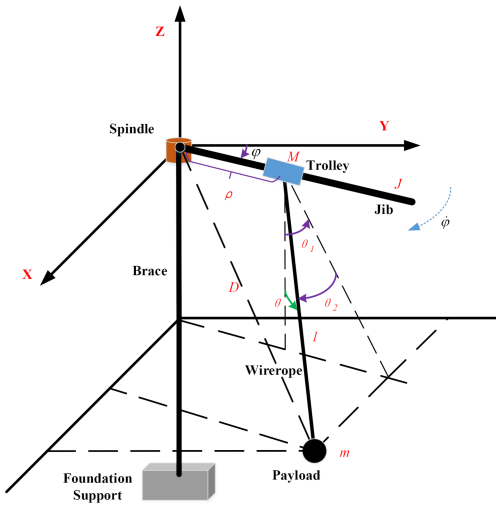

Fig. 1. A simplified model of payload swing of tower crane.

Table 1. Assumptions when constructing dynamic model of tower crane.

	Content
Assumption 1	Ignore the elasticity and quality of the wire rope transporting process
Assumption 2	Ignore the swing of the hoisting rope relative to the hook during the movement of the payload
Assumption 3	The deformation and vibration of the jib are ignored
Assumption 4	The payload is treated as a particle
Assumption 5	The rope length in three dimensions is approximately equal to the length of the swing rope in two dimensions

The dynamic model of the tower crane is very complicated. We consider the effect of various factors on payload swing. When constructing the tower crane dynamics model, this article made the following five assumptions in Table 1. In the three-dimensional model of the tower crane system, Table 2 shows the system parameters.

Based on the above 5 assumptions and according to the dynamic model of underactuated linkage system (where a<b) with a degree of freedom and b as the number of control variables, the classical dynamic model of tower crane based on the D'Alembert's principle and Euler-Lagrange's equation is established as follows [11]:

$$\boldsymbol{M}(\boldsymbol{q})\ddot{\boldsymbol{q}}+\boldsymbol{V}_m(\boldsymbol{q},\dot{\boldsymbol{q}})\dot{\boldsymbol{q}}+\boldsymbol{G}(\boldsymbol{q})=\boldsymbol{U}+\boldsymbol{F}_d. \tag{1}$$

Among them, $\boldsymbol{q}\in\mathbf{R}^{4\times1}$ represents the state vector of the system; $\boldsymbol{M}(\boldsymbol{q})\in\mathbf{R}^{4\times4}$ represents the inertia matrix; $\boldsymbol{V}_m(\boldsymbol{q},\dot{\boldsymbol{q}})\in\mathbf{R}^{4\times4}$ represents the direction Centripetal - Coriolis force matrix; $\boldsymbol{G}(\boldsymbol{q})\in\mathbf{R}^{4\times1}$ represents the gravity vector of the system; $\boldsymbol{U}\in\mathbf{R}^{4\times1}$ represents the control vector of the system; $\boldsymbol{F}_d\in\mathbf{R}^{4\times1}$ represents the system's friction disturbance vector.

Table 2. Tower crane system parameters.

Symbol	Implication	Unit
ρ	Variable amplitude motion displacement	m
φ	The angle of the jib	deg
θ_1	The swing angle of the payload in the vertical plane of the jib	deg
θ_2	The swing angle of the payload outside the vertical plane of the jib	deg
θ	The swing angle of the payload relative to the vertical direction	deg
l	The length of the rope	m
J	The moment of inertia of the jib	kg·m^2
M	Trolley mass	kg
m	Payload and hook mass	kg
D	The displacement of the payload with respect to the origin	m

The above quantities are specified as follows:

System state vector

$$\boldsymbol{q}=[\rho(t),\varphi(t),\theta_1(t),\theta_2(t)]^{\mathrm{T}}, \tag{2}$$

Inertia matrix of the system:

$$\boldsymbol{M}(\boldsymbol{q})=\begin{bmatrix} M+m & 0 & ml\cos\theta_1 & 0 \\ 0 & J+(M+m)\rho^2 & 0 & ml\rho\cos\theta_2 \\ ml\cos\theta_1 & 0 & ml^2 & 0 \\ 0 & ml\rho\cos\theta_2 & 0 & ml^2 \end{bmatrix}. \tag{3}$$

System Centripetal-Coriolis force matrix:

$$\boldsymbol{V}_m(\boldsymbol{q},\dot{\boldsymbol{q}})=\begin{bmatrix} 0 & 0 & -ml\dot{\theta}_1\sin\theta_1 & 0 \\ 0 & 0 & 0 & -ml\rho\dot{\theta}_2\sin\theta_2 \\ 0 & 0 & 0 & 0 \\ 0 & 0 & 0 & 0 \end{bmatrix}. \tag{4}$$

System gravity vector:

$$\boldsymbol{G}(\boldsymbol{q})=\begin{bmatrix} 0 & 0 & mgl\sin\theta_1 & mgl\sin\theta_2 \end{bmatrix}^{\mathrm{T}}. \tag{5}$$

System control vector:

$$\boldsymbol{U}=\begin{bmatrix} F_\rho & T_\varphi & 0 & 0 \end{bmatrix}^{\mathrm{T}}. \tag{6}$$

System friction disturbance vector:

$$\boldsymbol{F}_d=\begin{bmatrix} -f & -T_f & 0 & 0 \end{bmatrix}^{\mathrm{T}}. \tag{7}$$

According to the friction model in reference [11], the following friction model is selected to represent the fric-

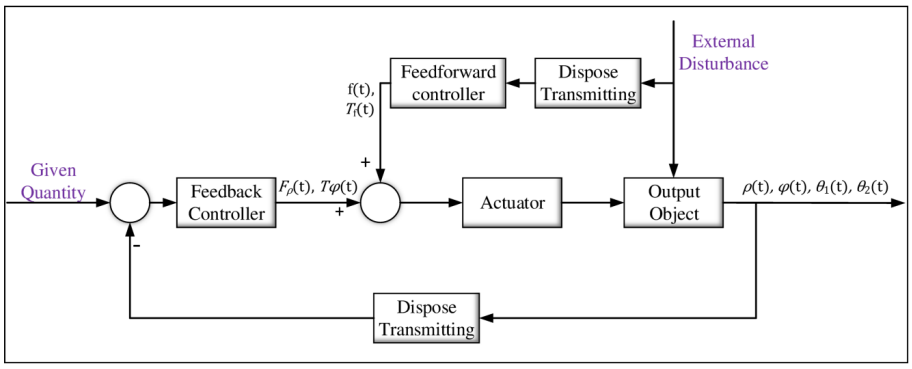

Fig. 2. Schematic diagram of overall control structure of tower crane.

tion characteristics of tower crane when transporting payload.

$$\begin{cases} f = f_{k0\rho}\tanh\dfrac{\dot{\rho}}{\mu} - f_{k1\rho}\,|\dot{\rho}|\,\dot{\rho}, \\ T_f = f_{k0\varphi}\tanh\dfrac{\dot{\varphi}}{\varepsilon} - f_{k1\varphi}\,|\dot{\varphi}|\,\dot{\varphi}. \end{cases} \tag{8}$$

In addition to the parameters already introduced above, in the above formulas, f and T_f in $\boldsymbol{F}_d$ respectively represent the control force for controlling the forward and backward movement of the trolley and the control torque force for controlling the rotation of the swing jib; and in are resistances in both directions. Among them, $f_{k0\rho}$, μ, $f_{k1\rho}$, $f_{k0\varphi}$, ε, $f_{k1\varphi} \in \mathrm{R}$ are corresponding friction factors.

To make the analysis clearer, the dynamic model established above is expanded as follows:

$$\begin{cases} (M+m)\ddot{\rho} + ml\ddot{\theta}_1\cos\theta_1 - ml\dot{\theta}_1^2\sin\theta_1 \\ \quad = F_\rho - f, \\ ml\ddot{\rho}\cos\theta_1 + mgl\sin\theta_1 + ml^2\ddot{\theta}_1 = 0, \\ J\ddot{\varphi} + (M+m)\rho^2\ddot{\varphi} - ml\rho\ddot{\theta}_2\cos\theta_2 \\ \quad - ml\rho\dot{\theta}_2^2\sin\theta_2 = T_\varphi - T_f, \\ ml\rho\ddot{\varphi}\cos\theta_2 + mgl\sin\theta_2 + ml^2\ddot{\theta}_2 = 0. \end{cases} \tag{9}$$

Fig. 2 shows the control structure schematic diagram for the tower crane dynamic model in this paper.

Remark 1: Considering the actual working conditions, the payload will not swing above the tumult, so the swing angles of $\theta_1(t)$ and $\theta_2(t)$ are always in the range $(-\pi/2,\ \pi/2)$. The mathematical expression is as follows:

$$-\frac{\pi}{2} < \theta_1,\ \theta_2 < \frac{\pi}{2},\ \forall t \geq 0. \tag{10}$$

Remark 2: $\boldsymbol{M}(\boldsymbol{q})$ matrix is invertible and is positive definite symmetric matrix.

3. CONTROLLER DESIGN AND CLOSED-LOOP STABILITY ANALYSIS

The main content of this section is to design an improved energy-coupled controller for the tower crane, and verify the closed-loop stability of the system when the controller acts through the Lyapunov method and LaSalle invariance principle.

3.1. Controller design

As mentioned in the previous two sections, the control target is to reach the target position $(\rho_d,\ \varphi_d)$ quickly and accurately and effectively eliminate the payload swing angles θ_1, θ_2. Furthermore, design appropriate controllers around this goal.

According to (9), the accelerations of the trolley, the inner swing angle of the vertical plane of the jib, the rotation of the jib and the outer swing angle of the vertical plane of the jib are respectively:

$$\begin{cases} \ddot{\rho} = \dfrac{-l\ddot{\theta}_1}{\cos\theta_1} - g\tan\theta_1, \\ \ddot{\theta}_1 = \dfrac{F_\rho - f + ml\dot{\theta}_1^2\sin\theta_1 + (M+m)g\tan\theta 1}{ml\cos\theta_1 - \frac{(M+m)l}{\cos\theta_1}}, \\ \ddot{\varphi} = \dfrac{-l\ddot{\theta}_2}{\cos\theta_2} - \dfrac{g\tan\theta_2}{\rho}, \\ \ddot{\theta}_2 = \dfrac{T_\varphi - T_f + ml\rho\dot{\theta}_2^2\sin\theta_2 + \left[J+(M+m)\rho^2\right]\rho g\tan\theta_2}{ml\rho\cos\theta_2 - \frac{[J+(M+m)\rho^2]l}{\rho\cos\theta_2}}. \end{cases} \tag{11}$$

The above expressions of ρ, φ, θ_1, θ_2 are related to the order in which the four quantities are solved, and they can also be solved in different order. That is $\ddot{\rho}$, $\ddot{\varphi}$ can also be expressed as follows:

$$\begin{cases} \ddot{\rho} = \dfrac{F_\rho - f + ml\dot{\theta}_1^2\sin\theta_1 + ml\ddot{\theta}_1\cos\theta_1}{M+m}, \\ \ddot{\varphi} = \dfrac{T_\varphi - T_f + ml\rho\dot{\theta}_2^2\sin\theta_2 - ml\rho\ddot{\theta}_2\cos\theta_2}{J+(M+m)\rho^2}. \end{cases} \tag{12}$$

Since the energy of the system can reflect its motion state, according to the dynamic model of underactuated system of tower crane analyzed above, its energy can be obtained as follows [5,11]:

$$E(t)=\frac{1}{2}\dot{\boldsymbol{q}}^{\mathrm{T}}\boldsymbol{M}_c(\boldsymbol{q})\dot{\boldsymbol{q}}+mgl(1-\cos\theta_1\cos\theta_2), \tag{13}$$

where $\boldsymbol{M}_c=\boldsymbol{M}(\boldsymbol{q})$, the other quantities in the formula have the same meaning as in the previous section. And the energy function $E(t)$ is positive, that is, $E(t)\geq 0$.

For the energy formula, the derivative of time is substituted into equations (9), (11), (12), (13) and sorted out.

$$\dot{E}(t)=\dot{\boldsymbol{q}}^{T}(\boldsymbol{U}+\boldsymbol{F}_d)=(F_\rho-f)\dot{\rho}+(T_\varphi-T_f)\dot{\varphi}. \tag{14}$$

This formula indicates that the tower crane system with $\boldsymbol{U}+\boldsymbol{F}_d$ as input, $\boldsymbol{q}$ as output and $E(t)$ as energy storage function is passive and dissipative. But $\dot{E}(t)$ does not directly include the relevant information $\theta(t)$, $\dot{\theta}(t)$ in the payload. That is, the payload swing angles $\theta_1(t)$, $\theta_2(t)$ in the energy $E(t)$ of the underactuated system of the tower crane are not strongly coupled with the control input amount $\boldsymbol{U}+\boldsymbol{F}_d$. In order to enhance the state correlation between the payload status information and the input information. A new energy storage function needs to be constructed in the process of designing the controller of the system.

Modifying the energy function can enhance the coupling relationship between the indirectly controlled object and the directly controlled object in the underactuated system. To this end, the construction process of a new energy function is introduced next.

In order to construct a suitable energy function and controller, the error signals before the payload reaches the target position are defined as [24]:

$$\begin{cases}\rho_p=\rho(t)-\rho_d,\\ \varphi_p=\varphi(t)-\varphi_d.\end{cases} \tag{15}$$

According to the positional relationship of the payload swing angle, jib, and trolley in the three-dimensional space direction, we define the generalized positioning error signals after considered the coupling between them comprehensively.

$$\begin{cases}\sigma_\rho=\rho_p-k_{a\rho}\sin\theta_1,\\ \sigma_\varphi=\varphi_p-\dfrac{k_{a\varphi}\sin\theta_2}{\rho+k_{a\varphi}}.\end{cases} \tag{16}$$

Where $k_{a\rho}$, $k_{a\varphi}\in \mathrm{R}^+$ are positive control gains. And the denominator is not equal to 0.

It can be seen that the signal contains all the information of $\rho(t)$, $\varphi(t)$, $\theta_1(t)$, $\theta_2(t)$, and the derivative of the error signals in the above two directions is obtained.

$$\begin{cases}\dot{\sigma}_\rho=\dot{\rho}-k_{a\rho}\dot{\theta}_1\cos\theta_1,\\ \dot{\sigma}_\varphi=\dot{\varphi}+\dfrac{k_{a\varphi}\dot{\rho}\sin\theta_2}{(\rho+k_{a\varphi})^2}-\dfrac{k_{a\varphi}\dot{\theta}_2\cos\theta_2}{\rho+k_{a\varphi}}.\end{cases} \tag{17}$$

The control amount equivalently acts on the generalized rotary motion and generalized horizontal motion of the payload. In this way, the derivative of the constructed new energy storage function is as follows:

$$\dot{E}_t(t)=(F_\rho-f)\dot{\sigma}_\rho+(T_\varphi-T_f)\dot{\sigma}_\varphi. \tag{18}$$

After the construction of the energy storage function described above, the coupling between the quantities increases significantly. That is, the swing angle θ_1 has a nonlinear relationship with the displacement ρ of the trolley in the function of the generalized error signal, and the swing angle θ_2 has a nonlinear relationship with the turning angle φ of the jib and the displacement ρ of the trolley. Based on the constructed new energy storage function, consider the following formula for the positive definite scalar function $V(t)$.

$$V(t)=E_t(t)+\frac{k_{p\rho}{\sigma_\rho}^2}{2}+\frac{k_{p\varphi}{\sigma_\varphi}^2}{2}, \tag{19}$$

where $k_{p\rho}$, $k_{p\varphi}\in \mathrm{R}^+$ are positive control gains. $\dot{E}_t(t)=k_{p\rho}\sigma_\rho\dot{\sigma}_\rho+k_{p\varphi}\sigma_\varphi\dot{\sigma}_\varphi\geq 0$ is the derivative of the improved energy function. The derivative of

$$\dot{V}(t)=(F_\rho-f+k_{p\rho}\sigma_\rho)\dot{\sigma}_\rho+(T_\varphi-T_f+k_{p\varphi}\sigma_\varphi)\dot{\sigma}_\varphi. \tag{20}$$

The constructed controller is as follows based on the above form of $\dot{V}(t)$ and combine (9), (13), (14), (16), (18) to get

$$\begin{cases}F_\rho=-k_{p\rho}(\rho_p-k_{a\rho}\sin\theta_1)\\ \qquad -k_{d\rho}(\dot{\rho}-k_{a\rho}\dot{\theta}_1\cos\theta_1)+f,\\ T_\varphi=-k_{p\varphi}(\varphi_p-\dfrac{k_{a\varphi}\sin\theta_2}{\rho+k_{a\varphi}})\\ \qquad -k_{d\varphi}(\dot{\varphi}+\dfrac{k_{a\varphi}\dot{\rho}\sin\theta_2}{(\rho+k_{a\varphi})^2}-\dfrac{k_{a\varphi}\dot{\theta}_2\cos\theta_2}{\rho+k_{a\varphi}})+T_f.\end{cases} \tag{21}$$

Where $k_{d\rho}$, $k_{d\varphi}\in \mathrm{R}^+$ are the positive control gains.

The result of formula (21) is the nonlinear anti-sway control rate designed in this paper. The driving force F_ρ of the trolley movement and the driving torque force T_φ of the jib rotation are used as the design criteria as the input of the system. The real-time change of rope length is not considered here.

3.2. Closed-loop system stability analysis

Based on the design of the previous section, the adjustable control law of the stable payload movement can ensure that the positioning error of the trolley and the jib is gradually converged to zero. At the same time, during the transportation, the payload's swing angle swings within a small range and is eventually eliminated. That is, Theorem 1 must be satisfied.

Theorem 1: The controller (21) can drive the trolley and the jib to lift the payload accurately to the specified positions ρ_d, φ_d, and when the system is stable, the effective residual swing angle θ_1 and θ_2 of the load is effectively eliminated. In the sense that

$$\begin{aligned}&\lim_{t\to\infty}\left[\rho(t)\ \dot{\rho}(t)\ \varphi(t)\ \dot{\varphi}(t)\ \theta_1(t)\ \dot{\theta}_1(t)\theta_2(t)\ \dot{\theta}_2(t)\right]\\&=[\rho_d\ \ 0\ \ \varphi_d\ \ 0\ \ 0\ \ 0\ \ 0\ \ 0].\end{aligned}\tag{22}$$

Proof: To prove Theorem 1, we first define the following non-negative scalar function:

$$V(t)=E_t(t)+\frac{k_{p\rho}{\sigma_\rho}^2}{2}+\frac{k_{p\varphi}{\sigma_\varphi}^2}{2}\geq 0.\tag{23}$$

Combining formulas (19)-(21), derivate the scalar function $V(t)$.

$$\dot{V}(t)=-k_{d\rho}\dot{\sigma}_\rho^2-k_{d\varphi}\dot{\sigma}_\varphi^2\leq 0.\tag{24}$$

According to its derivative, it can be known that

$$V(t)\leq V(0),\ \forall t\geq 0.\tag{25}$$

That is, the equilibrium point of the closed-loop system is stable in the sense of Lyapunov, which is easy to obtain

$$V(t)\in L_\infty.\tag{26}$$

According to formula (20), (22) and (23), it can be obtained:

$$\begin{aligned}&\rho_p,\varphi_p,\rho,\varphi,\theta_1,\theta_2,\sigma_\rho,\sigma_\varphi,\dot{\sigma}_\rho,\dot{\sigma}_\varphi,\\&\dot{\rho},\dot{\varphi},\dot{\theta}_1,\dot{\theta}_2,F_\rho,T_\varphi\in L_\infty.\end{aligned}\tag{27}$$

For further prove the stability of the closed-loop signal and complete the proof of the whole theorem, the following set S is defined:

$$S=\left\{\left(\rho,\varphi,\dot{\rho},\dot{\varphi},\theta_1,\theta_2,\dot{\theta}_1,\dot{\theta}_2\right)\middle|\dot{V}(t)=0\right\}.\tag{28}$$

Define Ω as the largest invariant set in S. It is easy to know from formula (24) that in the set Ω, the derivative of the system's generalized positioning error signal:

$$\begin{cases}\dot{\sigma}_\rho=\dot{\rho}-k_{a\rho}\dot{\theta}_1\cos\theta_1=0,\\ \dot{\sigma}_\varphi=\dot{\varphi}+\dfrac{k_{a\varphi}\dot{\rho}\sin\theta_2}{(\rho+k_{a\varphi})^2}-\dfrac{k_{a\varphi}\dot{\theta}_2\cos\theta_2}{\rho+k_{a\varphi}}=0.\end{cases}\tag{29}$$

The following formula can be obtained:

$$\begin{cases}\sigma_\rho=\rho_p-k_{a\rho}\sin\theta_1=\alpha_\rho,\\ \sigma_\varphi=\varphi_p-\dfrac{k_{a\varphi}\sin\theta_2}{\rho+k_{a\varphi}}=\alpha_\varphi,\end{cases}\tag{30}$$

$$\begin{cases}\ddot{\sigma}_\rho=\ddot{\rho}-k_{a\rho}\ddot{\theta}_1\cos\theta_1-k_{a\rho}\dot{\theta}_1^2\sin\theta_1\\ \quad=0,\\ \ddot{\sigma}_\varphi=\ddot{\varphi}+\dfrac{k_{a\varphi}\ddot{\rho}\sin\theta_2+2k_{a\varphi}\dot{\rho}\dot{\theta}_2\cos\theta_2}{(\rho+k_{a\varphi})^2}\\ \qquad-\dfrac{2k_{a\varphi}\dot{\rho}^2\sin\theta_2}{(\rho+k_{a\varphi})^3}+\dfrac{k_{a\varphi}\ddot{\theta}_2\cos\theta_2}{\rho+k_{a\varphi}}-\dfrac{k_{a\varphi}\dot{\theta}_2^2\sin\theta_2}{\rho+k_{a\varphi}}\\ \quad=0.\end{cases}\tag{31}$$

In the above formulas, α_ρ and α_φ are undetermined constants. According to the formulas (21), (27), (28), (30), in the set Ω,

$$\begin{cases}F_\rho=-k_{p\rho}\alpha_\rho,\\ T_\varphi=-k_{p\varphi}\alpha_\varphi.\end{cases}\tag{32}$$

Assuming that $\alpha_\rho\neq 0$, we can see from Equation (31):

$$\dot{\rho}(t)=\begin{cases}-\infty,\ \alpha_\rho>0,\\ +\infty,\ \alpha_\rho<0,\end{cases}\ t\to\infty.\tag{33}$$

This is contradictory to the formula (27): $\dot{\rho}(t)\in L_\infty$, and the hypothesis does not hold. Combined with formula (12), if $\dot{\rho}(t)\in L_\infty$ and only if $\alpha_\rho=0$.

In summary, combined with formula (28)-(33), after analysis, in the set Ω,

$$\alpha_\rho=0,\ \ddot{\rho}=0,\ F_\rho=0.\tag{34}$$

$\dot{\rho}=\dot{\rho}_p=\beta,\ \beta\in\mathrm{R}$ is the undetermined constant. Similarly, make the same assumption, it is not difficult to obtain in the set Ω, if and only if $\beta=0,\ \ddot{\rho}=0$ holds, that is, $\dot{\rho}=\dot{\rho}_p=0$.

Combined with (23), (27), (28), (30) and (31). It is not difficult to draw

$$\theta_1=0,\ \dot{\theta}_1=0,\ \ddot{\theta}_1=0.\tag{35}$$

In the same way, it is similar to the above proof process, which will not be repeated here.

$$\alpha_\varphi=0,\ \ddot{\varphi}=0,\ T_\varphi=0.\tag{36}$$

From $\dot{\varphi}=\dot{\varphi}_p=0$,

$$\theta_2=0,\ \dot{\theta}_2=0,\ \ddot{\theta}_2=0.\tag{37}$$

It is easy to get from formulas:

$$\sigma_\rho,\sigma_\varphi,F_\rho,T_\varphi,\ddot{\rho},\ddot{\varphi}=0.\tag{38}$$

Substitute formulas (35) and (37) into (30) and (15), and combine formula (38). It is easy to know that $\sigma_\rho=0\to\rho-\rho_d$, $\sigma_\varphi=0\to\varphi(t)-\varphi_d$.

From the conclusions of formulas (34)-(38), it can be seen that the maximum invariant set Ω contains only one equilibrium point:

$$\left[\rho(t),\dot{\rho}(t),\varphi(t),\dot{\varphi}(t),\theta_1(t),\dot{\theta}_1(t),\theta_2(t),\dot{\theta}_2(t)\right]$$

$$= [\rho_d \quad 0 \quad \varphi_d \quad 0 \quad 0 \quad 0 \quad 0 \quad 0].$$

According to Russell's principle of invariance [23-25], the theorem is proved. That is for the following parameters:

$$\rho_p, \varphi_p, \rho, \varphi, \theta_1, \theta_2, \dot{\rho}, \dot{\varphi}, \dot{\theta}_1, \dot{\theta}_2.$$

Formula was established:

$$\lim_{t\to\infty} [\rho(t) \ \dot{\rho}(t) \ \varphi(t) \ \dot{\varphi}(t) \ \theta_1(t) \ \dot{\theta}_1(t) \ \theta_2(t) \ \dot{\theta}_2(t)]$$
$$= [\rho_d \quad 0 \quad \varphi_d \quad 0 \quad 0 \quad 0 \quad 0 \quad 0].$$

This is the end of proof. □

4. SIMULATION RESULTS AND EXPERIMENTAL ANALYSIS

In order to test the effectiveness and robustness of the control performance of the proposed control method shown in (21). This section is mainly carried out through experimental verification and simulation analysis on the tower crane experimental platform (See Fig. 3). Table 3 shows the given parameters of the experimental platform.

In Fig. 3, the forward and backward movement of the trolley is driven by an AC servo motor (trolley's control motor, 1500 W, 3000 r/min), and the horizontal displacement is obtained by a coaxial encoder (2000PPR) connected to the servo motor. The rotation of the jib is driven by the AC servo motor (1000 W, 3000 r/min) installed on the jib to drive the large gear connected to the column to complete the relative rotation. The rotation angle is obtained by the coaxial encoder (2000PPR) connected with

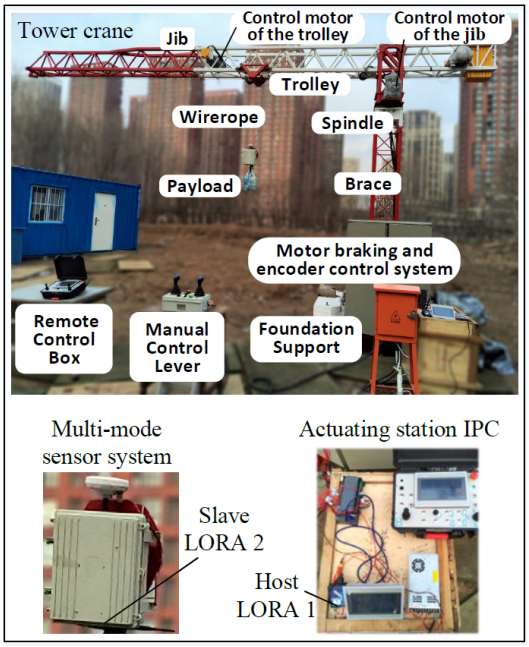

Fig. 3. Tower crane experiment platform.

Table 3. The given parameters of the experimental platform.

Symbol	Implication	Numerical value	Unit
J	The moment of inertia of the jib	300	$kg \cdot m^2$
M	Trolley mass	9	kg
g	Gravitational acceleration	9.8	m/s^2
L	Total horizontal length	6	m
H	Total vertical height	3.3	m
ρ_L	Trolley trip	5	m
ϕ_L	Rotation range of jib	±180	deg
l_L	Hook stroke	3	m
G_M	Maximum load	150	kg

the rotary servo motor. After the transformation, the rotation angle of the jib and the horizontal displacement of the trolley can be obtained. This position signal is collected and processed by the motion control board (high-speed DSP as the motion control core) in the motor braking and encoder control system, and then transmitted to the upper computer PC through the LORA (a type of wireless device) of the execution station IPC. After the position swing angle of the payload is collected and processed by the multimode sensor system (MPU6050 as the sensor of processing core), the data is uploaded to the upper PC by the wireless device LORA in the form of digital signal. In this way, the remote signal is transmitted to the upper computer. The host computer PC uses MATLAB/Simulink module to real-time window target. The PC generates control input commands according to the designed control law and transmits them to the execution station IPC through the wireless device LORA. The motion control board in the motor braking and encoder control system transmits the input commands to the two AC servo motors respectively, and the control cycle is 10 ms.

Specifically, the communication method of the tower crane automatic driving experiment platform is wired and wireless communication. The designed control law is realized by programming in C ++ language on PC. The control signal of the PC is sent out from the slave LORA 1 and received by the LORA 1 master. After the signal is processed by the execution station IPC, the motion control board in the motor braking and encoder control system sends the signal to the corresponding AC servo motor controller respectively. The controllers control the motors to take corresponding actions. At the same time, the payload position information collected and processed by the multimode sensor system is sent from the wireless slave LORA 2 to the wireless host LORA 2 connected to the host PC in real time. The PC stores the received hexadecimal data as a txt file in real time. A program written in MATLAB soft-

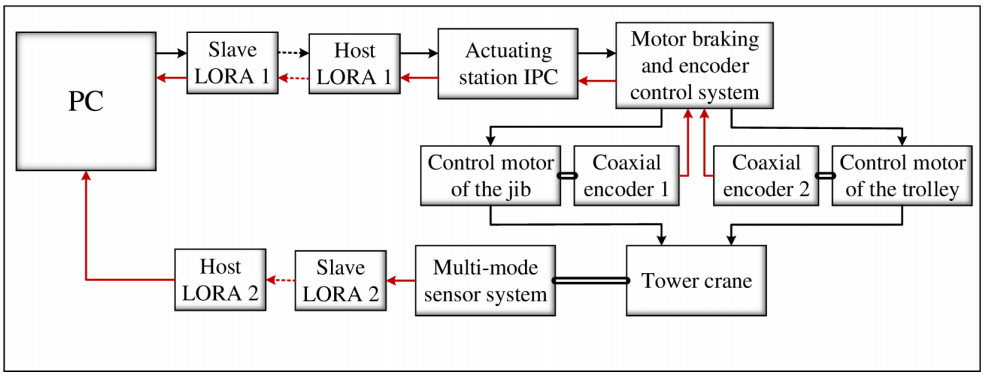

Fig. 4. Control mode of signal transmission logic diagram.

ware converts hexadecimal numbers to decimal numbers in real time and displays them in graphical form through MATLAB/Guide and MATLAB/Simulink modules. Fig. 4 is a logic diagram of signal transmission in the control mode (The direction of the arrow is the transmission direction of the signal flow. The solid line represents wired communication, and the dotted line represents wireless communication).

The main content of the experiment is to test the performance of the designed controller. It is specifically divided into:

1) Simulation comparison of control performance under precise model parameters.
2) Basic control performance experiment.
3) The robustness test of the control effect of the controller when the payload mass and the rope length change.
4) Robustness detection under uncertain parameters.
5) The robustness test when the external disturbances are added to the stability state.

In order to describe the distance and the payload's swing amplitude during the movement process, the following calculation formula is designed in this paper.

The distance of the payload from the origin on the central axis of the tower crane.

$$D = \sqrt{{x_q}^2 + {y_q}^2 + {z_q}^2}. \tag{39}$$

The displacements in the three directions of space:

$$\begin{cases} x_q = l\sin\theta_2 + (l\cos\theta_2\sin\theta_1 + \rho)\sin\varphi, \\ y_q = (l\cos\theta_2\sin\theta_1 + \rho)\cos\varphi, \\ z_q = -l\cos\theta_2\cos\theta_1. \end{cases} \tag{40}$$

The relationship between the pendulum's vertical swing angle and the two sub-direction swing angles:

$$l\cos\theta = l\cos\theta_2\cos\theta_1. \tag{41}$$

4.1. Comparison of basic control performance simulation

To verify the control effect of the controller proposed in this paper, we compared the classic LQR controller [10,24], PD controller [5] and adaptive trajectory tracking controller(ATTC) [24] in the modernized control theory after linearization.

The design of the PD controller is as follows:

$$\begin{cases} F_{\rho PD} = -k_{p1}(\rho - \rho_d) - k_{d1}\dot{\rho} + f, \\ T_{\varphi PD} = -k_{p2}(\varphi - \varphi_d) - k_{d2}\dot{\varphi} + T_f, \end{cases} \tag{42}$$

where $k_{p1}, k_{d1}, k_{p2}, k_{d2} \in \mathrm{R}^+$ are control gains. The control gains during comparison are consistent with the selection of the controller mentioned in this article.

In order to design the LQR controller, we linearized the model of the tower crane. The resulting LQR controller is as follows:

$$\begin{cases} F_{\rho LQR} = -k_{t1}(\rho - \rho_d) - k_{t2}\dot{\rho} - k_{t3}\theta_1 - k_{t4}\dot{\theta}_1, \\ T_{\varphi LQR} = -k_{j1}(\varphi - \varphi_d) - k_{j2}\dot{\varphi} - k_{j3}\theta_2 - k_{j4}\dot{\theta}_2, \end{cases} \tag{43}$$

where k_{t1}, k_{t2}, k_{t3}, k_{t4}, k_{j1}, k_{j2}, k_{j3}, $k_{j4} \in \mathrm{R}^+$ are control gains. The selection mode of control gains are determined by referring to reference [24] and after many times of debugging.

The design of the adaptive trajectory tracking controller(ATTC) is as follows:

$$\begin{cases} F_{\rho ATTC} = -k_{p1}(\rho - \rho_d) - k_{d1}\dot{\rho} \\ \qquad\qquad + (M+m)\ddot{\rho}_T + ml\dot{\theta}_1\cos\theta_1 \\ \qquad\qquad + f - \dfrac{2\lambda_{\omega\rho}{\xi_\rho}^2}{\left({\xi_\rho}^2 - (\rho - \rho_d)^2\right)^2}(\rho - \rho_d), \\ T_{\varphi ATTC} = -k_{p2}(\varphi - \varphi_d) - k_{d2}\dot{\varphi} \\ \qquad\qquad + (M+m)\ddot{\varphi}_T + ml\dot{\theta}_2\cos\theta_2 \\ \qquad\qquad + T_f - \dfrac{2\lambda_{\omega\varphi}{\xi_\varphi}^2}{\left({\xi_\varphi}^2 - (\varphi - \varphi_d)^2\right)^2}(\varphi - \varphi_d), \end{cases} \tag{44}$$

Table 4. Simulation parameters set during simulation.

Symbol	Implication	Numerical value	Unit
m	Payload and hook mass	2	kg
l	The length of the rope	1.2	m
ρ_d	The target position of the trolley	2.5	m
φ_d	The target position of the jib	120	deg
D_d	The target position of the payload with respect to the origin	2.77	m

where $k_{p1}, k_{d1}, k_{p2}, k_{d2} \in \mathrm{R}^+$ are control gains. ρ_T, φ_T are the target tracking trajectory, see [24] for specific planning methods and parameters, $\lambda_{\omega\rho}, \lambda_{\omega\varphi} \in \mathrm{R}^+$ are positive gains to be adjusted, and ξ_ρ, $\xi_\varphi \in \mathrm{R}^+$ are tracking in two directions respectively error limit value.

Set some parameters here as follows: $\lambda_{\omega\rho} = 0.1$, $\lambda_{\omega\varphi} = 0.1$, $\xi_\rho = 0.05$, $\xi_\varphi = 0.05$.

The parameters of the trolley, the target position, etc. in the system are set as Table 4.

The initial state of the system:

$\rho(0) = \varphi(0) = 0$, $\dot{\rho}(0) = \dot{\varphi}(0) = 0$, $\theta_1(0) = \theta_2(0) = 0$.

According to [22] and multiple simulation tests to get the best control performance, the selected control gain parameters after improvement are shown in Table 5. Figs. 5-7 show the simulation results. The control effect of the controller proposed in this article is indicated by red line, the control effect of the LQR controller in classic cybernetics is indicated by the purple dotted line, the control effect of the traditional PD controller is represented by the green dot-dash line, and the control effect of the adaptive trajectory tracking controller in classic cybernetics is indicated by the blue dotted line. Table 6 shows the evaluation indexes.

The meanings of the parameters defined in Table 6 are as follows:

t_{s1}: The time for the trolley to reach the setting destination.

t_{s2}: The time for the jib to reach the setting destination.

θ_{1m}: The maximum angle of θ_1.

θ_{2m}: The maximum angle of θ_2.

θ_m: The maximum angle of θ.

θ_s: Residual swing angle in the joint direction after running for 15 seconds.

t_a: Total time required for residual swing angle to meet industrial requirements.

F_m: Maximum driving force of the trolley during execution.

T_m: Maximum torsional driving force of the jib during execution.

From Figs. 5-7 and Table 6, it can be concluded that when the basic parameters are similar, the target position

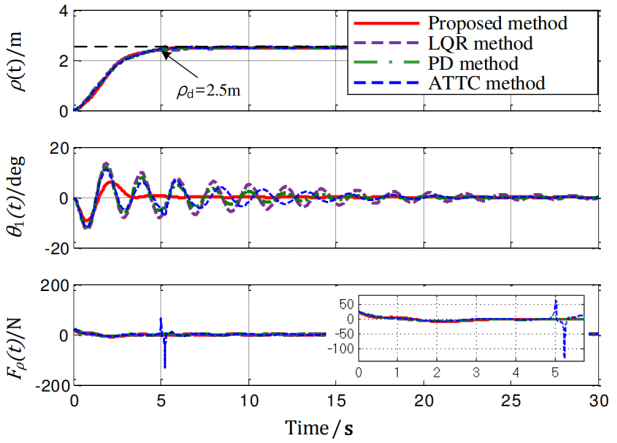

Fig. 5. Simulation results for proposed controller, LQR controller, PD controller and the adaptive trajectory tracking controller in the motion direction of the trolley.

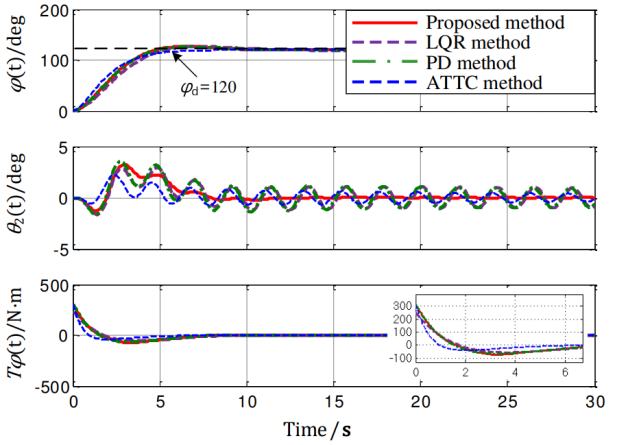

Fig. 6. Simulation results for proposed controller, LQR controller, PD controller and the adaptive trajectory tracking controller in the rotation direction of the jib.

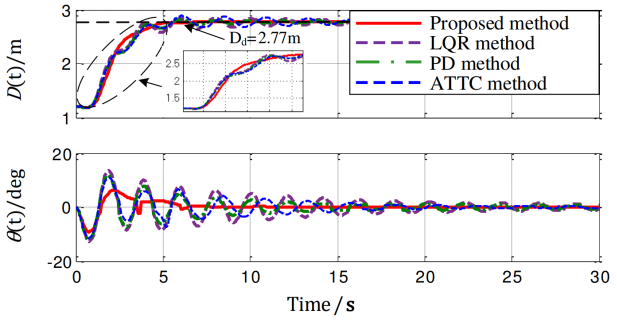

Fig. 7. Simulation results for proposed controller, LQR controller, PD controller and the adaptive trajectory tracking controller in the compound direction.

Table 5. Control gains for two controllers.

Controllers	$k_{p\rho}$	$k_{a\rho}$	$k_{d\rho}$	$k_{p\varphi}$	$k_{a\varphi}$	$k_{d\varphi}$	k_{t1}	k_{t2}	k_{t3}	k_{t4}	$f_{k0\rho}$	$f_{k1\rho}$
Proposed method	10	1	20	152	1	323	NA	NA	NA	NA	6	8
LQR	NA	NA	NA	NA	NA	NA	11	20	3	2	6	8
PD	NA	NA	NA	NA	NA	NA	NA	NA	NA	NA	6	8
ATTC	NA	NA	NA	NA	NA	NA	NA	NA	NA	NA	6	8
Controllers	$f_{k0\varphi}$	$f_{k1\varphi}$	μ	ε	k_{j1}	k_{j2}	k_{j3}	k_{j4}	k_{p1}	k_{d1}	k_{p2}	k_{d2}
Proposed method	6	1	1	1	NA	NA	NA	NA	NA	NA	NA	NA
LQR	6	1	1	1	221	302	4	1.5	NA	NA	NA	NA
PD	6	1	1	1	NA	NA	NA	NA	NA	NA	NA	NA
ATTC	6	1	1	1	NA	NA	NA	NA	10	20	152	323

Table 6. Controller simulation comparison evaluation indicators.

Controllers	$t_{s1}(s)$	$t_{s2}(s)$	$\theta_{1m}(deg)$	$\theta_{2m}(deg)$	$\theta_m(deg)$
Proposed method	4.72	5.05	6.12	3.24	6.04
LQR	5.50	6.72	13.85	7.23	13.72
PD	5.21	5.12	13.70	4.72	13.62
ATTC	4.93	5.15	13.25	2.45	13.12
Controllers	$\theta_s(deg)$	$t_a(s)$	$F_m(N)$	$T_m(N.m)$	
Proposed method	0	7.20	24.2	318	
LQR	5.12	>25	25	461	
PD	5.06	>25	26.2	321	
ATTC	2.12	>25	125	319	

is the same, the method proposed in this article in terms of the maximum driving force F_m and the maximum torsional driving force T_m are the least compared to the other three methods, the tower crane system under the action of the proposed controller in this article performs best. The controller proposed in this paper effectively restrains the load from swinging in two directions, and the residual swing angle is quickly eliminated when it reaches the setting destination. In particular, the controller designed in this paper has the least time to reach the target position, the elimination time $t_a = 7.2$ s of the residual swing angle, the smallest swing angle θ_{1m}, θ_m, of the motion direction and the combined direction. Although in the rotation direction of the jib, the adaptive trajectory tracking controller has the smallest angle θ_{2m}, the swing angle in the merging direction is still larger than the method in this paper, and the adaptive trajectory tracking method has a great impact on the system at the fifth second. Compared with the three control methods, the proposed controller improves the control performance.

4.2. Basic control performance experiment

In order to verify the control performance of the proposed controller in the experimental application process, we compared the experimental results with the simulation results. Running the experiments under the above parameters of Experiment 4.1, the results obtained are shown in Figs. 8-10. The red solid line represents the simulation result graph, and the experimental measurement graph is represented by the blue dashed line.

It can be seen from Figs. 8-10 that the experimental results have basically the same effect as the simulation under the proposed controller. The reason for the slight difference between the two curves is the influence of the hardware conditions of the system (rotation of the motor, elongation of the wirerope, etc.) on the control accuracy during the experimental control. The trolley accurately reached the target position $\rho_d = 2.5$ m in about 5 s. At the same time, the swing jib reached the target position $\varphi_d = 120$ degrees at about 5 s. The distance between the payload and the origin on the central axis of the tower crane reached the position $D_d = 2.77$ m accurately in about 5s. And in this process, the amplitude of the swing angle θ_1 of the rope did not exceed 7 degrees. The amplitude of the swing angle θ_2 of the hanging rope did not exceed 4 degrees. The amplitude of the swing angle θ of the suspended rope relative to the vertical direction did not exceed 8 degrees. At the same time, when the target position is reached, swing angle of payload in all directions quickly converge to zero, and the residual swing is eliminated in a little while. This shows that the control law designed in this paper effectively suppressed the load swing angle during transportation. The controller has good anti-swing transient control performance.

4.3. Impact of payload mass and rope length changes on robustness

To test the robustness of the designed control law, three sets of control variable experiments were performed in this experiment and compared with the basic control performance experiment of Experiment 4.2. Figs. 11-13 show the simulation results (Experimental testing is not done here).

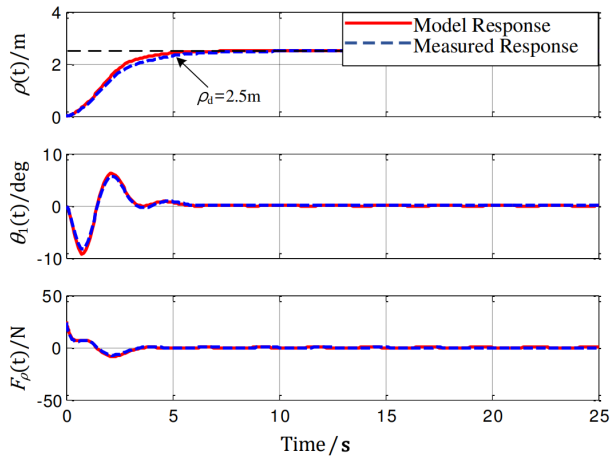

Fig. 8. Results for proposed controller in the motion direction of the trolley on basic control performance comparison test.

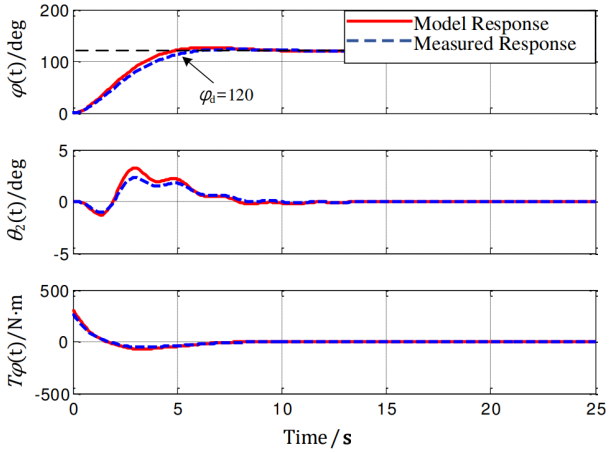

Fig. 9. Results for proposed controller in the rotation direction of the jib on basic control performance comparison test.

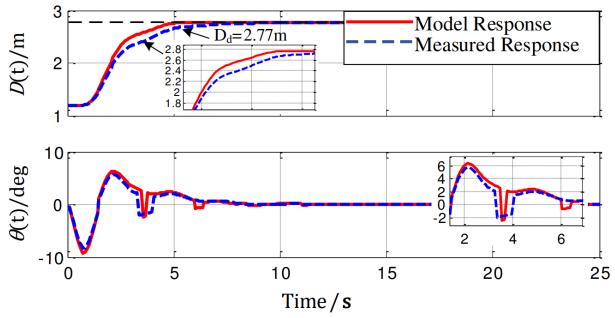

Fig. 10. Results for proposed controller in the compound direction on basic control performance comparison test.

Case 1: Compared with Experiment 4.2, only the payload mass was changed to $m = 22$ kg, and other parameters were the same as Experiment 4.2. The simulation results are shown by the blue dotted lines in Figs. 11-13.

Case 2: Compared with Experiment 4.2, only the length of the hanging rope was changed to $l = 2.5$ m, and other parameters were the same as Experiment 4.2. The simulation results are shown by the green dashed lines in Figs. 11-13.

Case 3: Compared with Experiment 4.2, the Parameter changes are $m = 22$ kg, $l = 2.5$ m, respectively. The simulation results are shown by the purple dotted lines in Figs. 11-13.

Figs. 11-13 show the simulation results of the three cases. It can be seen from the above simulation result graph that, whether it is Case 1 changing the payload mass or Case 2 changing the length of the sling, or Case

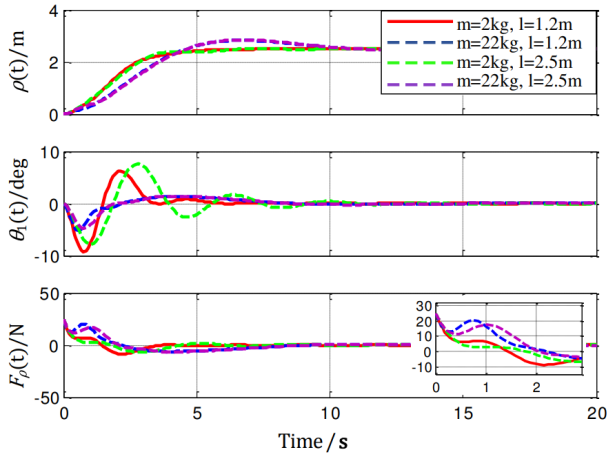

Fig. 11. Simulation results for proposed controller in the motion direction of the trolley.

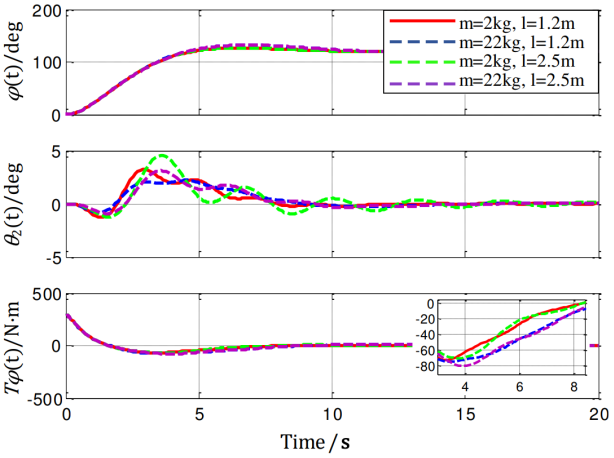

Fig. 12. Simulation results for proposed controller in the rotation direction of the jib.

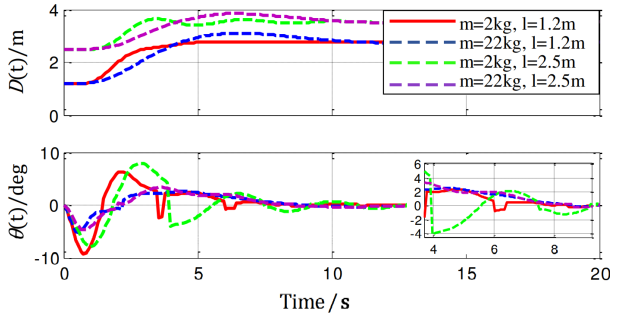

Fig. 13. Simulation results for proposed controller in the compound direction.

3 the payload mass and the length of the sling simultaneously change. The control law designed in this paper can achieve the same control effect as that of Experiment 4.2. When the rope length and load quality are changed, the load reaching the target position in both directions t_{s1} and t_{s2} are basically controlled within 10 s; the maximum synthetic swing angle θ_m during the process is controlled within 9 degrees, or even smaller; the swing angle is basically eliminated within 2 s. This shows that the control law designed in the article has the advantages of good control performance and adaptability, and good robustness.

4.4. Impact of target position changes on robustness

In order to verify the dynamic response performance of the control scheme under the condition of uncertain parameters, this simulation experiment compared four different cases. Four different target locations were selected:

1) $\rho_d = 2.5$ m, $\varphi_d = 120$ degrees;
2) $\rho_d = 1.5$ m, $\varphi_d = 120$ degrees;
3) $\rho_d = 2.5$ m, $\varphi_d = 135$ degrees;
4) $\rho_d = 1.5$ m, $\varphi_d = 135$ degrees;

Figs. 14-16 show the simulation results (Experimental testing is not done here). It can be seen from the simulation results in Fig. 14-16 that the control law designed in this paper can achieve the same good control effect as Experiment 4.2 when the transport target position changes under four conditions. It can accurately and quickly transport the payload to the setting destination. When the target position changes, the swing angle θ_{1m} and θ_{2m} of the load in the two directions during the whole lifting process is within 4 degrees and 9 degrees respectively; the time t_{s1} to reach the target position is controlled within 5s; when the target position is reached, the residual swing angle θ tends to 0 degree. This indicates that the control scheme has excellent dynamic response performance and good control robustness under uncertain parameters.

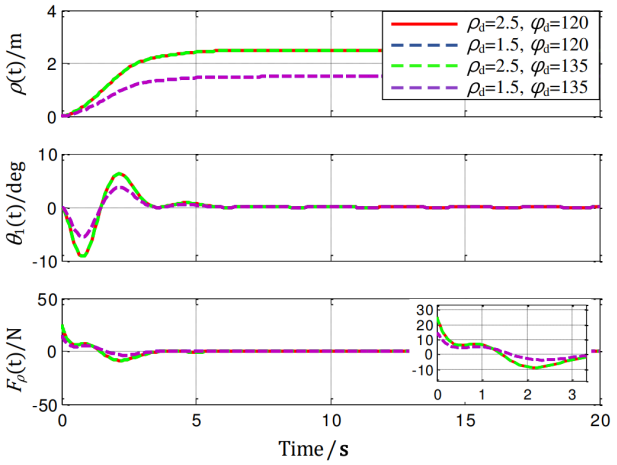

Fig. 14. Simulation results of different target locations for proposed controller in the motion direction of the trolley.

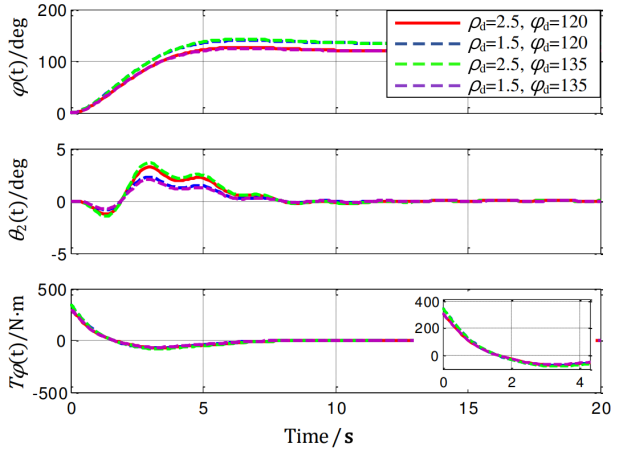

Fig. 15. Simulation results of different target locations for proposed controller in the rotation direction of the jib.

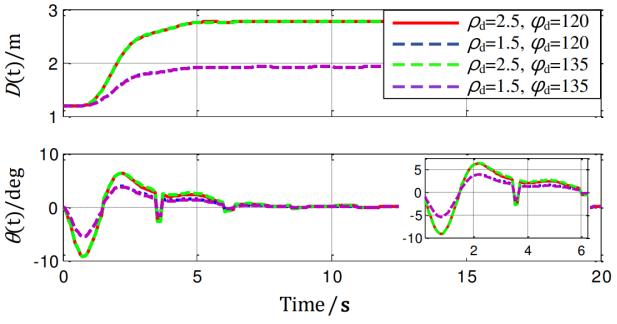

Fig. 16. Simulation results of different target locations for proposed controller in the compound direction.

4.5. Experiment on the influence of disturbance on controller robustness

When a tower crane is transporting a payload, external disturbances such as wind payloads and collisions are inevitable. To test the robustness of the control law against external interference, the content of this experiment is to add external disturbances to simulate the wind payload when the payload reaches a stable state, and observe whether the payload can reach the steady state again and the time required to reach the steady state. The added external interference is to be similar to the actual working environment, and the added interference is limited to within 10 degrees. The parameters of this experiment are the same as those of the basic control performance test of Experiment 4.2. The difference is that at 11 s, when the payload reaches the equilibrium state, a 1.5-degree sinusoidal trigonometric function disturbance is added to the two directions. The experimental results of the test are in Figs. 17-19. The red solid line represents the simulation result graph, and the experimental measurement graph is represented by the blue dashed line.

Figs. 17-19 show the experimental results have basically the same effect as the simulation under the proposed controller when interference is added. The reason for the slight difference between the two curves is the same as Experiment 4.2. In addition, when adding disturbances to the payload, there is an error from the theoretically designed disturbances. Therefore, the curves are not overlap. It can be clearly seen that under the action of forces and moments in two directions of the control law F_ρ, T_φ. After the trolley, swing jib, and payload reach the designated position accurately and the swing angle stabilizes, external disturbance factors are added at 11 s. Under the action of the controller, the change in the trolley's displacement and the jib's angle is very weak, and the swing angle of the payload in both directions can still be quickly stabilized within 6 s. The change of the swing angle θ_1 of the payload is controlled within 4 s, and the swing angle becomes stable within 6 s. The residual swing angle approaches 0 within 7 s. The displacement change does not exceed 0.6 m. The change of the swing angle θ_2 of the payload is controlled within 4.5 s, and the residual swing angle meets the swing amplitude requirement within 5 s. The rotation angle of the jib does not change more than 15 degrees. After synthesis, the amplitude of the swing angle θ of the sling relative to the vertical direction is 17 degrees, and the residual swing meets the swing amplitude requirement within 7 s and is finally eliminated, and the combined direction of displacement change does not exceed 0.97 m.

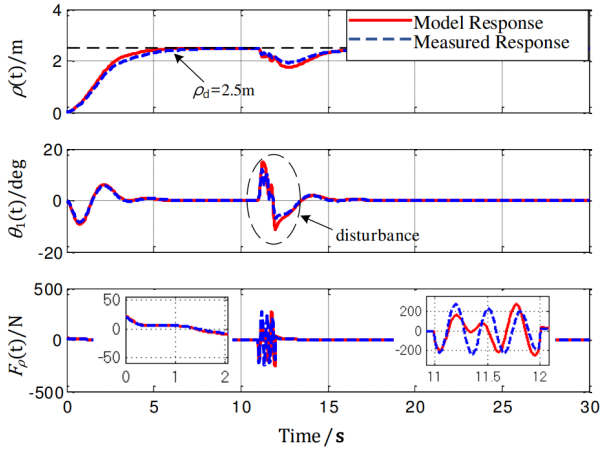

Fig. 17. Results for proposed controller in the motion direction of the trolley when adding external disturbances.

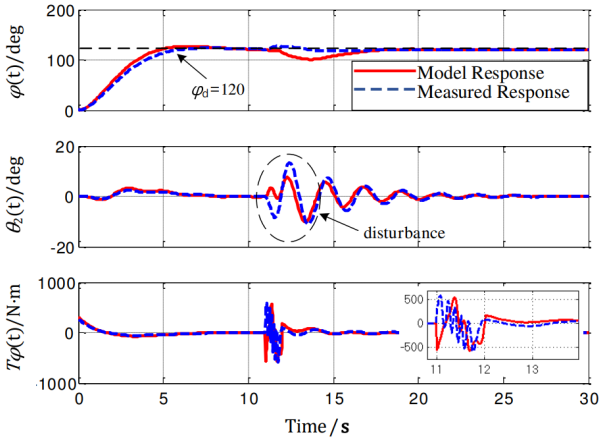

Fig. 18. Results for proposed controller in the rotation direction of the jib when adding external disturbances.

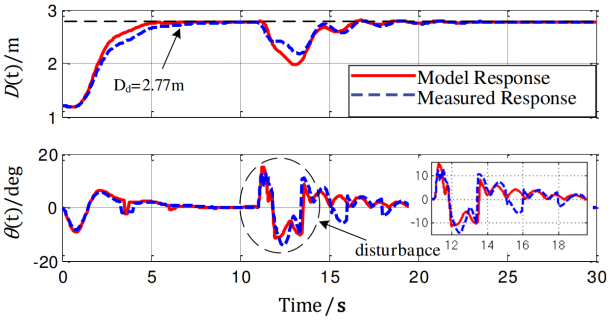

Fig. 19. Results for proposed controller in the compound direction when adding external disturbances.

5. CONCLUSION

To solve the problems of poor positioning accuracy, large amplitude of payload swing and poor anti-

interference performance for underactuated tower crane system, an improved energy coupling anti-swing control method is proposed in this article. A controller based on the improved energy function is designed, which considered the the strong coupling of trolley movement and payload swing, jib rotation and payload swing. The proposed controller achieved the maximum swing angle of 6.04 degrees under 5 seconds and effective suppression and elimination of residual swing angle. Compared with the traditional LQR controller, PD controller, and the adaptive trajectory tracking controller in the transportation efficiency, the proposed controller has been greatly improved by at least 50%. In terms of driving force, suppression of swing amplitude, and elimination of residual swing angle, the proposed controller has the best control effect. When the length of the suspension rope and the payload mass change, the designed controller still meets the requirements, the swing amplitude is controlled within 7 degrees or even smaller, and the effective suppression and elimination of the residual swing angle are within 5 s. In addition, the proposed controller has the same control effect under the condition of uncertain parameters. It has good robustness and continues to stabilize by maintaining the internal swing angle of 3 s when external disturbance is added. The experimental results applied on the experimental platform have the same control effect as the simulation analysis. The proposed control method provides a theoretical basis for the anti-sway control of the tower crane and helps to improve the working efficiency of tower crane.

REFERENCES

[1] N. Sun, Y. M. Wu, H. Chen, and Y. C. Fang, "Antiswing cargo transportation of underactuated tower crane systems by a nonlinear controller embedded with an integral term," *IEEE Transactions on Automation Science and Engineering*, vol. 16, no. 3, pp. 1387-1398, January 2019.

[2] J. MatusKo, S. Iles, F. Kolonic, and V. Lesic, "Control of 3D tower crane based on tensor product model transformation with neural friction compensation," *Asian Journal of Control*, vol. 17, no. 2, pp. 443-458, September 2014.

[3] S. Garrido, M. Abderrahim, A. Gimenez, and R. Diez, "Anti-swinging input shaping control of an automatic construction crane," *IEEE Transactions on Automation Science and Engineering*, vol. 5, no. 3, pp. 549-557, July 2008.

[4] M. H. Korayem, A. Zehfroosh, H. Tourajizadeh, and S. Manteghi, "Optimal motion planning of non-linear dynamic systems in the presence of obstacles and moving boundaries using SDRE: Application on cable-suspended robot," *Nonlinear Dynamics*, vol. 76, no. 2, pp. 1423-1441, April 2014.

[5] H. T. Shi, G. Li, X. Ma, and X. T. Bai, "Research on nonlinear coupling anti-swing control method of double pendulum gantry crane based on improved energy," *Symmetry*, vol. 11, no. 12, pp. 1511, December 2019.

[6] D. I. Martinez, J. D. J. Rubio, T. M. Vargas, V. Garcia, and A. Carlos, "Stabilization of Robots with a Regulator Containing the Sigmoid Mapping," *IEEE Access*, vol. 8, no. 1, pp. 89479-89488, 2020.

[7] M. X. Hou and H. T. Shi, "The Adaptive distributed event-triggered observer approach to cooperative output regulation of discrete-time linear multi-agent systems under directed switching networks," *IEEE Access*, vol. 8, pp. 221568-221579, December 2020.

[8] J. D. J. Rubio, G. Ochoa, M. V. Dante, G. Enrique, and J. Novoa, "Structure regulator for the perturbations attenuation in a quadrotor," *IEEE Access*, vol. 7, no. 1, pp. 138244-138252, September 2019.

[9] S. Alvarez-Rodrguez and G. Flores, "PID principles to obtain adaptive variable gains for a bi-order sliding mode control," *International Journal of Control, Automation, and Systems*, vol. 18, no. 10, pp. 2456-2467, October 2020.

[10] T. A. Le, S. G. Lee, and S. C. Moon, "Partial feedback linearization and sliding mode techniques for 2D crane control," *Transactions of the Institute of Measurement and Control*, vol. 36, no. 1, pp. 78-87, January 2014.

[11] N. Sun, Y. C. Fang, and X. B. Zhang, "Energy coupling output feedback control of 4-DOF underactuated cranes with saturated inputs," *Automatica*, vol. 49, no. 5, pp. 1318-1325, May 2013.

[12] H. T. Shi and X. T. Bai, "Model-based uneven loading condition monitoring of full ceramic ball bearings in starved lubrication," *Mechanical Systems and Signal Processing*, vol. 139, pp. 106583, May 2020.

[13] H. M. Omar and A. H. Nayfeh, "Gain scheduling feedback control for tower cranes," *Journal of Vibration and Control*, vol. 9, no. 3-4, pp. 399-418, January 2003.

[14] M. X. Hou and H. T. Shi, "Stator-winding incipient shorted-turn fault detection for motor system in motorized spindle using modified interval observers," *IEEE Transactions on Instrumentation and Measurement*, vol. 70, November 2020.

[15] H. M. Omar and A. H. Nayfeh, "Anti-swing control of gantry and tower cranes using fuzzy and time-delayed feedback with friction compensation," *Shock and Vibration*, vol. 12, no. 2, pp. 73-89, May 2005.

[16] L. Vermeiren, A. Dequidt, and M. Afroun, "Motion control of planar parallel robot using the fuzzy descriptor system approach," *ISA Transactions*, vol. 51, no. 5, pp. 596-608, September 2012.

[17] A. Gonzlez, V. Estrada-Manzo, and T. M. Guerra, "Gain-scheduled H_∞ admissibilisation of LPV discrete-time systems with LPV singular descriptor," *International Journal of Systems Science*, vol. 48, no. 15, pp. 3215-3224, September 2017.

[18] A. Gonzlez and T. M. Guerra, "Enhanced predictor-based control synthesis for discrete-time TS fuzzy descriptor systems with time-varying input delays," *IEEE Transactions on Fuzzy Systems*, vol. 27, no. 2, pp. 402-410, February 2019.

[19] J. Vaughan, D. Kim, and W. Singhose, "Control of tower cranes with double-pendulum payload dynamics," *IEEE Transactions on Control Systems Technology*, vol. 18, no. 6, pp. 1345-1358, November 2010.

[20] S. C. Duong, E. Uezato, H. Kinjo, and T. Yamamotoc, "A hybrid evolutionary algorithm for recurrent neural network control of a three-dimensional tower crane," *Automation in Construction*, vol. 23, pp. 55-63, May 2012.

[21] T. S. Wu, M. Karkoub, W. S. Yu, T. H. Chien, G. W. Ming, and W. Kuan, "Anti-sway tracking control of tower cranes with delayed uncertainty using a robust adaptive fuzzy control," *Fuzzy Sets and Systems*, vol. 290, pp. 118-137, May 2016.

[22] T. S. Wu, M. Karkoub, H. Wang, S. C. Ho, and H. Ti, "Robust tracking control of MIMO underactuated nonlinear systems with dead-zone band and delayed uncertainty using an adaptive fuzzy control," *IEEE Transactions on Fuzzy Systems*, vol. 25, no. 4, pp. 905-918, August 2017.

[23] L. Liu, Y. J. Dapeng, S. C. Tong, and Z. S. Wang, "Barrier Lyapunov function-based adaptive fuzzy FTC for switched systems and its applications to resistance-inductance-capacitance circuit system," *IEEE Transactions on Cybernetics*, vol. 50, no. 8, pp. 3491-3502, 2020.

[24] H. Chen, Y. C. Fang, and N. Sun, "An adaptive tracking control method with swing suppression for 4-DOF tower crane systems," *Mechanical Systems and Signal Processing*, vol. 123, pp. 426-442, May 2019.

[25] N. Sun, Y. C. Fang, H. Chen, and B. Lu, "Slew/translation positioning and swing suppression for 4-DOF tower cranes with parametric uncertainties: Design and hardware experimentation," *IEEE Transactions on Industrial Electronics*, vol. 63, no. 10, pp. 6407-6418, July 2016.

[26] S. C. Moon, W. G. Lee, and S. G. Lee, "Adaptive sliding mode control of overhead cranes with varying cable length," *Journal of Mechanical Science and Technology*, vol. 27, no. 3, pp. 885-893, March 2013.

[27] L. Tang, D. Ma, and J. Zhao, "Adaptive neural control for switched non-linear systems with multiple tracking error constraints," *IET Signal Processing*, vol. 13, no. 3, pp. 330-337, 2018.

[28] S. G. Lee, L. C. Nho, and D. H. Kim, "Model reference adaptive sliding mode control for three dimensional overhead cranes," *International Journal of Precision Engineering and Manufacturing*, vol. 14, no. 8, pp. 1329-1338, August 2013.

[29] V. A. Le, H. X. Le, L. Nguyen, and X. P. Minh, "An efficient adaptive hierarchical sliding mode control strategy using neural networks for 3D overhead cranes," *International Journal of Automation and Computing*, vol. 16, no. 5, pp. 614-627, April 2019.

[30] H. Coral-Enriquez, S. Pulido-Guerrero, and J. Corts-Romero, "Robust disturbance rejection based control with extended-state resonant observer for sway reduction in uncertain tower-cranes," *International Journal of Automation and Computing*, vol. 16, no. 6, pp. 812-827, May 2019.

[31] A. A. El-Badawy and M. M. G. Shehata, "Anti-sway control of a tower crane using inverse dynamics," *Proc. of IEEE International Conference on Engineering and Technology (ICET)*, 19-20 April 2014, pp. 1-6.

[32] F. N. Koumboulis, N. D. Kouvakas, G. L. Giannaris, and D. Vouyioukas, "Independent motion control of a tower crane through wireless sensor and actuator networks," *ISA Transactions*, vol. 60, pp. 312-320, January 2016.

[33] G. Lee, H. H. Kim, C. J. Lee, S. I. Ham, S. H. Yun, H. Cho, B. K. Kim , G. T. Kim , and K. Kim, "A laser-technology-based lifting-path tracking system for a robotic tower crane," *Automation in Construction*, vol. 18, no. 7, pp. 865-874, November 2009.

[34] M. Bock and A. Kugi, "Real-time nonlinear model predictive path-following control of a laboratory tower crane," *IEEE Transactions on Control Systems Technology*, vol. 22, no. 4, pp. 1461-1473, September 2013.

Huaitao Shi received his B.S. and Ph.D. degrees in control engineering from Northeastern University, Shenyang, China, in 2005 and 2012, respectively. He has been a Professor with the Faculty of Mechanical Engineering, Shenyang Jianzhu University, Shenyang, where he has also been the Vice Dean, since 2014. He is the author of more than 40 articles, (26 articles were indexed by SCI), and six patents. His current research interest includes research on nonlinear underactuated system and hybrid ceramic ball-bearing.

Jianqi Huang was born in Chengde, Hebei, in 1994. He received his B.S. degree in mechanical engineering from University of Jinan, Jinan, China, in 2018. He is currently pursuing a master's degree in mechanical engineering with the School of Mechanical Engineering, Shenyang Jianzhu University, Shenyang, China. His research interest is automatic control of underactuated cranes.

Xiaotian Bai was born in Wanghua, Fushun, Liaoning, China, in 1989. He received his B.S. degree in mechanical engineering from the Dalian University of Technology, Dalian, in 2011, and his M.S. and Ph.D. degrees in mechanical engineering from the Shenyang University of Technology, in 2013 and 2016, respectively. He has been an Assistant Professor with the faculty of Mechanical Engineering, Shenyang Jianzhu University, Shenyang, China, since 2019. His current research interest is about the establishment of kinetic model and the vibration and sound radiation of bearings.

Xiang Huang received his B.S. degree in computer science and technology from Nanjing University of Information Science and Technology in 2007, an M.S. degree in applied computer science from Nanjing University of Aeronautics and Astronautics in 2010, and a Ph.D. degree in mechanical engineering from South China University of Technology in 2013. He worked as an Assistant Professor in Zhejiang University of Technology between 2014 and 2020. His current research interest is about computational modeling and optimization of porous structures.

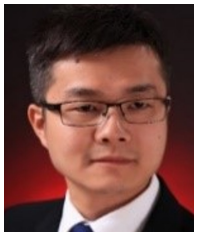

Jie Sun received his B.S. and Ph.D. degrees from Northeastern University, Shenyang, China, in 2005 and 2011, respectively. He has been an Assistant Professor with the State Key Laboratory of Rolling Technology and Continuous Rolling Automation, Northeastern University, Shenyang. He is the author of more than 50 articles, (24 articles were indexed by SCI). His current research interest includes research on R & D of continuous rolling process simulation and automatic control technology.